Local measurements of wildland fire dynamics in a field-scale experiment

Local measurements of wildland fire dynamics in a field-scale experiment

ERIC V. MUELLER[1*], NICHOLAS SKOWRONSKI[2], JAN C. THOMAS[1], KENNETH CLARK[2], MICHAEL GALLAGHER[2], RORY M. HADDEN[1], WILLIAM MELL[2], ALBERT SIMEONI[3,1]
[1]School of Engineering, University of Edinburgh, Edinburgh, UK
[2]USDA Forest Service, Morgantown, WV, New Lisbon, NJ, Newtown Square, PA, and Seattle, WA, USA
[3]Worcester Polytechnic Institute, Worcester, MA, USA
**Corresponding author*: e.mueller@ed.ac.uk

Abstract
Local point measurements of fire dynamics in field-scale experiments of wildland fires are highly useful. This is true both for understanding the mechanisms driving fire spread that result in the observed macroscopic behaviors, but also in terms of providing comparison points for numerical tools, such as detailed physics-based fire behavior models. This work describes measurements of temperature, velocity, and radiative heat flux that were made in a field-scale fire experiment in a pine forest, with the aim of providing both of the above benefits. Regions of both surface fire and crown fire were captured and are compared. The crown fire exhibited tall upright flames, compared to the shorter tilted flames of the surface fire. Crown fire resulted in a significant increase in integrated radiative preheating, by a factor of ~1.75, as well as greater flow sheltering in the downstream region of the fire front. Further, a corrective factor is introduced for oblique sensor placement relative to the fire front, in order to improve the value of these and other measurements, particularly for model comparison. The presented methodology, while able to be improved, is shown to successfully characterize local differences in fire behavior.

Keywords: *wildland fires; fire dynamics; fire spread; field experiment*

1. Introduction
In the study of wildland fire dynamics, local measurements of fundamental physical phenomena can be highly valuable in providing insight into the global, or macroscopic, behavior observed. The importance of these measurements is magnified when they are intended for the testing and development of physics-based fire behavior models. As these models aim to resolve the underlying physics [1], any assessment of model capabilities benefits significantly from such measurements [2]. Therefore, this work aims to add to the available set of such measurements, using a simple but robust methodology.

Conventional theory of wildland fire spread identifies three distinct stages: preheating, flaming, and intermittent flaming and smoldering combustion (e.g. [3]). These stages can be quantified through thermodynamic measurements. Specifically, in this case, we consider measurements of temperature, velocity, and radiative heat flux. To start, gas-phase temperature has a long history in the study of fire science and fire behavior [4], and it can help reveal details of flame spread, flame and plume geometry, and fire-induced turbulence. Flow velocity also provides information on the flame and plume dynamics as well as interactions with the ambient wind [5–7]. And finally, radiative heat flux gives an indication of the intensity of preheating associated with the fire front [8]. While convective heat flux can also be important (whether through heating or cooling) [9], it is not directly a feature of the fire front itself, unlike the other chosen variables. The rate of convective heating to a fuel element is a function of the boundary layer (both velocity and temperature) which forms around the element, as well as the temperature of the element itself [10]. This makes direct measurement of magnitudes related to vegetation elements difficult. However, a sense of the tendency for heating or cooling potential, as well as data for numerical modeling, can be obtained from the gas-phase temperature and velocity measurements. Overall, these three measurements help to understand the nature of energy

transfer and oxygen availability, which are necessary to sustain the combustion reaction, and which must be properly represented in a physics-based model of fire spread.

A number of previous field experiments have investigated some combination of the aforementioned measurements [9,11–20]. These have been conducted in a variety of ecosystems, ranging from grassland [15,18,20], to shrubland [14,16,19], to forests [9,11,12,17]. However, measurement techniques are not typically consistent, and the level of detail provided on the macroscopic fire behavior (e.g. fuel structure and consumption, fire progression), varies significantly. This level of detail is particularly important for the utility of such measurements in terms of both understanding fire behavior and testing numerical models.

To address this need, a collection of wildland fire behavior measurements was obtained during a field-scale experimental fire in the Pinelands National Reserve (PNR). Details of the ecosystem, as well as macroscopic features of fire behavior for the experiment are reported by Mueller et al. [21]. Sites of co-located measurements of temperature, velocity, and radiative heat flux were established, to be within the fire environment at flame level. This was specifically aimed at testing detailed physics-based fire models, as fire behavior will inevitably vary locally throughout a field experiment. Providing a variety of different measurements at the same location means that multiple aspects of the representation of the highly coupled physical phenomena can be evaluated at the same instant. Likewise, by linking these measurements to the global trends of fire progression, a more complete picture of fire behavior can be created.

2. Methods

2.1. Study site

The experiment was conducted in the Pinelands National Reserve (PNR) of New Jersey, USA. The site was a pitch-pine scrub-oak forest, dominated in the canopy by pitch pine (*Pinus rigida Mill.*), with intermittent clusters of post-oak (*Quercus stellata Wangenh.*) and white oak (*Quercus alba L.*) in the sub-canopy. The understory contained a shrub layer of huckleberry (*Gaylussacia spp.*), blueberry (*Vaccinium spp.*), and scrub oaks (*Quercus spp.*).

The measurements discussed here were conducted in the second of two experimental fires, carried out in March of 2014 (EX2 in Mueller et al. [21]). Surface fuels, forest floor and shrub layer, were destructively sampled at 36 pre- and post-fire sample locations. Average initial loading of thin fuel (assumed to contribute to fire spread) was 1.68 ± 0.42 kg·m^{-2}. Additionally, pre-fire litter depth ($n = 55$) was 5 ± 2 cm and the shrub layer height ($n = 120$) was 79 ± 19 cm. The forest canopy was characterized with pre- and post-fire airborne Light Detection and Ranging (LiDAR). This was calibrated to estimate fuel bulk density on a 3-dimensional grid with a 10 m x 10 m x 1 m resolution. Average initial loading of thin canopy fuel was 0.98 ± 0.20 kg·m^{-2} More details of the study site, including fuel structure, can be found in Mueller et al. [21].

Local fire behavior, the focus of this investigation, was measured at three sites. These were selected based upon an exploratory survey of the burn block. Locally homogenous density of the shrub layer (based on visual inspection) and avoidance of any direct contact with canopy branches were the two criteria used. The location of these sites (referred to as F1, F2, and F3) are shown in relation to the burn block perimeter and progression of the fire front in Fig. 1.

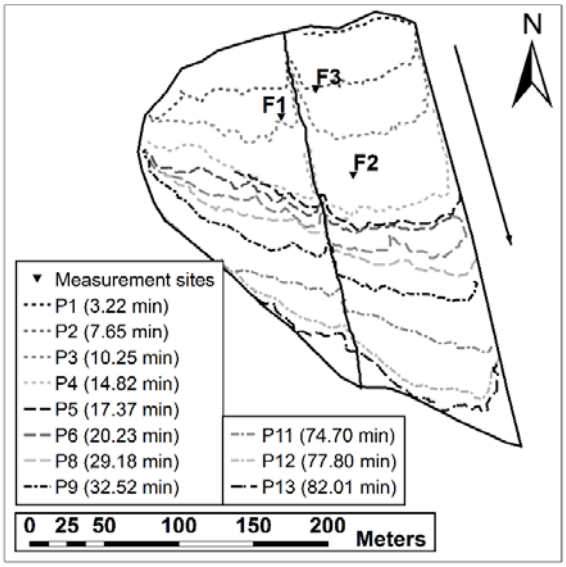

Fig. 1. Positioning of fire measurement sites in the experimental block. Isochrones P1-13 show the progression of the fire.

2.2. Instrumentation

Observation of the fire front progression was carried out with an aircraft-mounted IR and visual camera. This yielded the isochrones shown in Fig. 1. Additionally, ambient weather conditions, including wind at roughly canopy height (12.5 m), were monitored at a site ~100 m to the west of the experimental block. More details related to the macroscopic observation of fire behavior can be found in Mueller et al. [21].

Each local measurement site within the block consisted of one ‘primary’ tower, measuring gas-phase temperature, and sites F1 and F2 had three ‘secondary’ towers, measuring radiative heat flux and flow velocity (Fig. 2). The primary towers were placed upstream in the anticipated direction of fire spread so that they would be impacted first. This allowed a simultaneous measurement of the environment within the flames and the impact ahead of the front.

All sensors were recorded at a frequency of 50 Hz. This is greater than the response time of any particular sensor, as discussed below, but helps ensure that no high frequency fluctuations are not missed simply due to data acquisition techniques. Nevertheless, discussion is largely focused on events and trends that are on a time scale on the order of fire residence time. The data loggers (CR3000, Campbell Scientific) were placed in waterproof boxes and buried at each site, downstream of the anticipated direction of fire spread. This was done to avoid local effects on fire behavior in the measurement area due to disturbance of the vegetation.

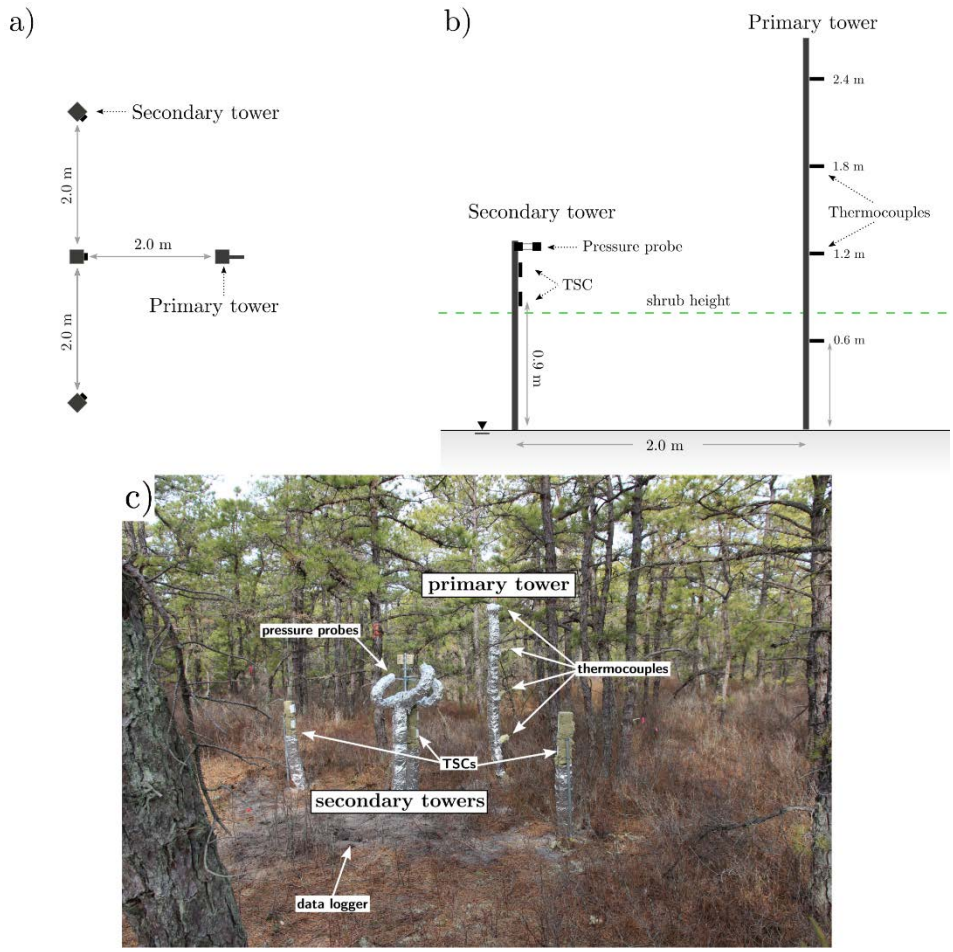

Fig. 2. Configuration of instrument array for fire behavior measurement, shown in (a) plan view, (b) section view, and (c) in-situ.

2.2.1. Temperature

On each of the primary towers, temperature measurements were made with four thermocouples placed vertically at 60 cm intervals, putting the lowest thermocouple below the average shrub layer height (Fig. 2b). The thermocouples were K-type, sheathed and grounded, having an outer sheath diameter of 0.25 mm (KMTXL-IM025G-150, Omega). The sheaths were insulated by ceramic tubes (ORM-11618-6, Omega), and the leads and connections were protected in a wrapping of mineral wool. Steel guy-wires were used to anchor the tower, in order to minimize oscillations and vibrations.

A particular source of errors in temperature measurements in fires is related to radiation gains and losses from thermocouples [4]. In this case, a small diameter was chosen not only to minimize response time (~0.2 s), but also to reduce errors related to radiative exchanges. Silvani and Morandini [22] gave an analysis of the potential for radiative errors in both the preheating and flame region for a number of relevant flow velocities for wildland fires, using similar sized thermocouples. They found that errors were <10%, so while the effect is considered in measurement error bars, no systematic corrections are applied to the measurements reported here.

2.2.2. Velocity

On the center secondary tower, flow velocity was measured with differential pressure sensors, or bi-directional McCaffrey probes [23]. Three of these were used, positioned at a height of 1.2 m (Fig. 2). They were oriented to be mutually orthogonal, particularly to characterize differences in horizontal versus vertical flow.

These probes operate by recording a pressure differential between two ports (one static and one dynamic, depending on flow direction), which is converted to a gas velocity based on the following:

$$u = \frac{1}{K}\sqrt{\frac{2\Delta P}{\rho}}, \quad (1)$$

where K is a correction factor and a temperature-dependent air density (ρ) is used. The probes have an inner opening diameter of 14.5 mm. A correction factor of 1.08 was used for these probes after wind tunnel calibration tests (Young Calibration Ltd.). This factor has been found to vary on the order of ±5% for individual probes, but this variability is considered acceptable given the numerous other sources of uncertainty. Plastic tubing, wrapped in an insulating layer of mineral wool, was used to connect the probes to differential pressure transducers (5266 DPT, Gems Sensors and Controls). The response time of these transducers is ~1 s. Due to the linear pressure-voltage response, but the non-linear nature of Eq. (1), the resolution of the sensors becomes increasingly coarse for low (ambient) flow velocities. Additionally, their signal response to off-axis velocity vectors does not have an ideal match to a cosine law [23,24], and, despite the orthogonal orientation of the three probes, a true 3-dimensional flow vector cannot be accurately quantified. Nevertheless, these probes are the current standard for flow measurement within the combustion environment in large-scale fire testing, particularly owing to their robustness (e.g. [18]). As reference temperature measurements at the location of the probes were unavailable, the measurements from the thermocouple at 1.2 m on the primary tower (shifted in time to account for the spread of the fire) were used to calculate gas density. This introduced some uncertainty to peak values (where temperature is high and gas density is low) but less so for lower-temperature entrainment flow, and the characteristics of flow direction are unaffected.

2.2.3. Radiative heat flux

On all three secondary towers, incident radiant heat fluxes were measured using thin-skin calorimeters (TSCs) [25]. Six of these were used per site, with two on each secondary tower at heights of 0.9 m and 1.1 m. The sensor faces were aimed at the primary tower to cover a wider total view angle, due to the uncertainty inherent in the actual angle of approach of the fire front (Fig. 2a). Each was comprised of a small stainless steel disk (diameter: 9.6 mm; thickness: 1.3 mm), fixed to the face of a square of ceramic insulation board. Thermocouple wires were welded to the back face of the disk, and the disk was painted black in order to maximize its absorptivity/emissivity (we assume $\alpha = \varepsilon = 1$). Employing a series of assumptions and laboratory calibrations (discussed below), it is possible to use the disk temperature measurements in order to solve an energy balance for the metal element, which in turn yields a calculation of incident radiative heat flux [26]. Chosen for their simplicity and affordability, these sensors have demonstrated prior utility in fire testing scenarios at both bench scale [27,28] and large scale [29]. Similar devices have also been tested in scenarios related to wildland fires [30,31].

The incident radiative flux on the TSCs is derived from the steel disc temperature, considering the element to be thermally-thin. Losses by conduction into the insulation are considered to be a proportion, C, of the received radiation, and using an energy balance the following equation for incident radiation is obtained [26]:

$$q''_{inc} = \frac{1}{\alpha(1-C)}\left[\gamma\frac{m}{A_s}c_p\frac{dT_s}{dt} + \varepsilon\sigma({T_s}^4 - {T_\infty}^4) - h_c(T_s - T_g)\right], \quad (2)$$

with the factor γ added to account for the tendency for overestimation in highly transient stages of heating (LHS of Eq. (2) is large). The sensors deployed in this experiment were calibrated in laboratory tests at the University of Edinburgh, using an automated movable radiant panel that allows

the specification of automated heating curves [26]. In this environment, the convective heat coefficient, h_c, was determined based on a correlation for natural convection over a flat vertical plate [10]. The calibration yielded the following empirical factors:

$$C(T_s) = 0.583 - 7.1 \cdot 10^{-4} \cdot T_s, \quad \gamma = 0.6, \tag{3}$$

with C as a function of disk temperature (°C). However, the long duration of the calibration tests (on the order of 100 min) is not indicative of the kinds of residence times typically encountered in wildland fires [11,17,32]. Therefore, shorter tests, with more rapid heating rates, were carried out to check the response of the sensors and the validity of the correction factors. This revealed a tendency for over-prediction of radiant flux in the short-term transient stages of heating. In fact, neglecting the use of any correction factors appears to give a better result in these conditions. It is hypothesized that this behavior is a function of the differing thermal response characteristics between the insulation board material and the stainless steel, which leads to the potential for near-zero conductive losses. Given that the short-term tests are more representative of the expected conditions in a wildland fire, any subsequent analysis of incident flux from the TSC measurements will use these two assumptions (corrected and uncorrected) as upper and lower error bounds. More details of the sensor calibration can be found in Mueller [33].

Finally, in the case of the experimental measurements, the surrounding environment differs from the quiescent laboratory, and so the convective coefficient in Eq. (2) was estimated using a Reynolds-based correlation for forced convection [10]:

$$h_c = \frac{\overline{Nu}_L k_f}{L} = \frac{k_f}{L}\left(0.664 {Re_L}^{1/2} {Pr_f}^{1/3}\right), \tag{4}$$

with gas-phase properties evaluated at the film temperature ($T_f = (T_g + T_s)/2$). This information is not directly available for every sensor, but an estimate can be made from the velocity measurements and the reference temperatures used to calculate the velocity. While this approach introduces uncertainties, it is deemed acceptable as we only consider heat flux measurements up to the time of the fire arrival at the primary tower (before the fire reaches the sensors, and convective effects become very significant).

3. Results and Discussion

3.1. Fire behavior overview

The fire was ignited by drip torch along the north edge of the experimental block, with the fire spreading as a linear front to the south. The flame front progressed predominantly as a surface fire, with some isolated regions of passive crown fire activity. Fire spread was roughly consistent with the ambient wind, which was measured to be 3.9 ± 1.8 m·s^{-1} at 12.5 m. For the period impacting the measurement sites (up to P4 in Fig. 1), mean spread rates along the front, determined from the aerial imagery, were 0.13-0.19 m·s^{-1}. Across the entire block, an average of 72% of surface fuels, or 1.21 kg·m^{-2}, and an average of 19% of canopy fuels, or 0.19 kg·m^{-2}, were consumed. Assuming an approximate value for the heat of combustion of vegetation, total fireline intensity was on the order of 4 MW·m^{-1}, during the period of interest. A more detailed analysis of the general fire behavior, including fuel structure and consumption is presented by Mueller et al. [21]. However, in order to give context to the measurements discussed here, characteristics specific to individual measurement sites are discussed.

Videos were available at sites F1 and F2, and from the recordings, a clear difference in behavior can be seen (Fig. 3). F1 exhibits a surface fire behavior with occasional torching. Flames are relatively

low (1-3 m), with some tilt and forward bursts. At F2, flames are taller (4-12 m, extending into the crowns) and more upright, particularly in the area leading up to the site. In both cases, the fire approaches the measurement site as a largely continuous linear front. Upon arrival, a greater fire depth is also observed at F2. Using the aerial visual imagery, fire depths were estimated to be ~5, 10, and 6 m for the three sites, respectively.

Fig. 3. Video stills from site (a-b) F1 and (c-d) F2. Images correspond to roughly (a,c) 30 s before fire arrival and (b,d) the time of fire arrival at the primary tower.

Using a combination of aerial infrared imagery and the point measurements of temperature, estimates of local spread rate were obtained. A value of 0.19 $m \cdot s^{-1}$, 0.40 $m \cdot s^{-1}$, and 0.15 $m \cdot s^{-1}$ was found for F1, F2, and F3, respectively. Likewise, changes in LiDAR-based canopy bulk density (CBD) can be used to compare the sites [21]. At F1, the pre-fire forest canopy was shorter, with most fuel below 10 m, and the peak CBD at 5-6 m. On the other hand, F2 and F3 show taller canopies (up to ~12 m), with peak CBD at 6-7 m (Fig. 4). Despite the greater similarity between the initial structure in F2 and F3, the consumption shows a more consistent fire behavior between F1 and F3. In these cases, consumption is generally concentrated below 7 m, averaging 0.05 $kg \cdot m^{-3}$ and 0.04 $kg \cdot m^{-3}$ along height, respectively. These profiles appear consistent with a surface fire exhibiting occasional torching/ladder fuel consumption. In contrast, consumption at F2 extended up to 10 m, averaging 0.08 $kg \cdot m^{-3}$. Perhaps more telling is the significant reduction in the variation of CBD at F2 (shaded region), suggesting a greater extent to the flames (e.g. crowning behavior) in this region, as observed in the video footage (Fig. 3). Given the higher spread rate and greater fuel consumption at F2, fireline intensity is estimated to be at least 15 $MW \cdot m^{-1}$, 3.75 times the previous estimate for the average during the period of interest (more representative of F1 and F2). Values may be even greater for the limited regions where total consumption of small diameter crown fuel was observed, but this is not fully captured by the LiDAR [21].

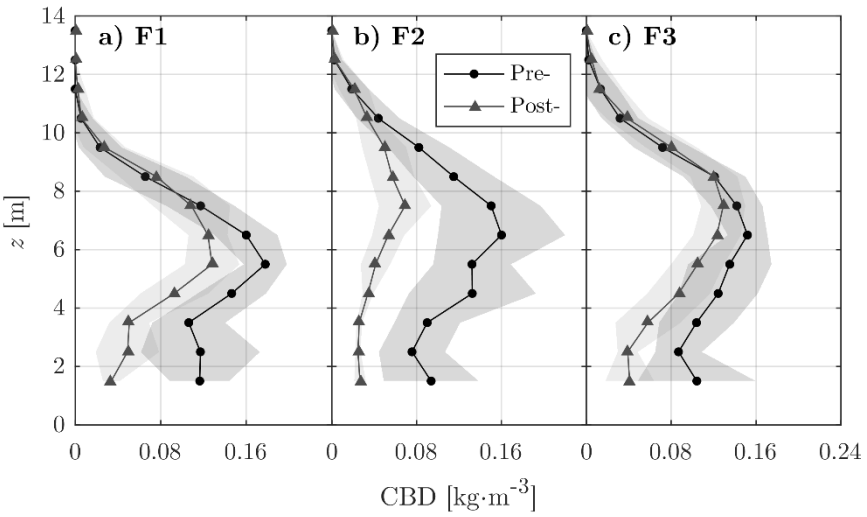

Fig. 4. Pre- (circles) and post-fire (triangles) average profiles of thin fuel CBD at (a) F1, (b) F2, and (c) F3. Average values (symbols) and standard deviations (shaded region) are taken over a 30 x 30 m region containing a given site.

3.2. Temperature

From the gas-phase time-temperature curves the three regions of preheating, flaming, and smoldering combustion can be examined at each site. As an example, instantaneous signals from the lowest (0.6 m) thermocouple are reported for each site in Fig. 5. Following previous studies [11,17,18,22], a flame-tip temperature of 300 °C is assumed, based on past field measurements [34]. In order to filter out short-lived peaks close to this threshold value, a 1-second moving average is applied to the instantaneous data for the purposes of this calculation. The first and last temperature in excess of the threshold are taken as the bounds of the flaming period (gray region in Fig. 5).

When using temperature measurements, the height of the sensor is an important factor. Not only will the flame depth generally diminish with height, but intermittent flaming at the surface can persist well after the passage of the fire front, particularly for larger (thicker) fuel elements. Temperature-based evaluations of the fire front will inevitably also depend on factors like sensor response time, sampling frequency, and signal processing. However, by establishing a fixed procedure for analysis, direct comparisons can be made between different measurements and the numerical predictions. Evaluation from the video proved difficult in this case owing to the angle of approach and the obscuration of view by flames.

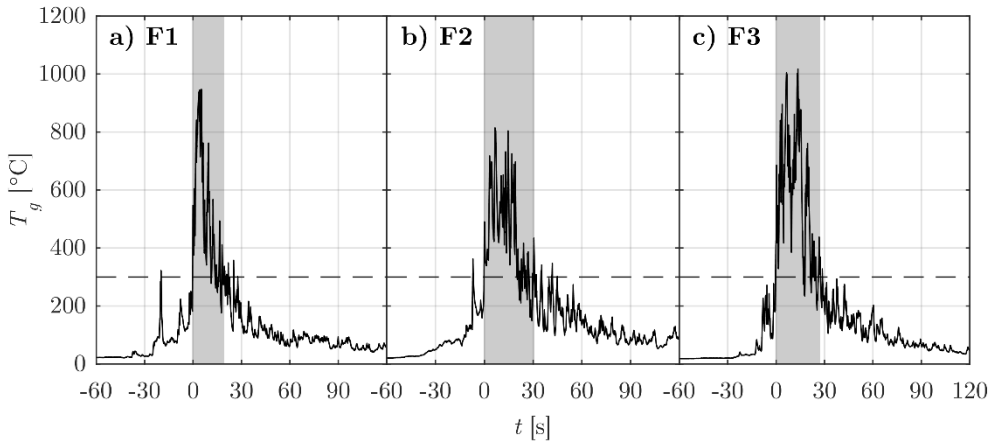

Fig. 5. Instantaneous gas-phase temperature at z = 0.6 m at sites (a) F1, (b) F2, and (c) F3. The gray region corresponds to the time between the first and last temperature exceeding 300 °C, from a 1-second moving average (residence time, t_r). Time is given relative to fire arrival at the primary tower.

In each case, temperatures during the preheating stage remain generally low with only one or two very short-lived peaks up to 200-300 °C. These are associated with bursts of hot gas ahead of the fire front and last no more than 10 seconds (with continuous pulses above 200 °C lasting no more than 2 seconds). The onset of the flaming stage is marked by a very rapid rise in temperature, consistent with expectations [12]. Temperatures remain elevated until the later stages of the flaming period, at which point they decay more gradually and with a significant amount of turbulent fluctuation. The intermittent flaming and smoldering combustion which follow, along with residual heat in the surface, contribute to continued turbulent updrafts in the wake of the front.

Information on the flaming period for all thermocouple heights is contained in Table 1. Peak temperatures are between 664 and 1017 °C, consistent with the range of roughly 600–1300 °C observed in a number of other studies including surface/shrub [16–18,22], and crown [12] fires. Fig. 6 shows the height dependency of peak temperature more clearly. This includes the estimated maximum under-prediction of temperature in the flame due to radiative losses (taken as 10% following Silvani and Morandini [22]). For sites F1 and F3, the highest peak temperature is at the lowest thermocouple with a clear decay along height, a result of the shrub-based surface fire observed in these locations (e.g. Fig. 3a-b). At F2, the highest peak temperature is actually at a height of 1.2 m, but the spread between peak values along height is less. A relatively constant temperature along height suggests all thermocouples were within the continuous, or persistent flame region [35].

Residence times are all between 17 – 34 s, though values at the lowest thermocouple should be more representative of the actual fire front residence time and are between 20 – 31 s. Longer times were found at F2, with the more intense fire behavior. The estimates of local spread and depth from Section 3.1 give residence times of 26, 25, and 40 s for the three sites respectively. These compare relatively well at F1 and F2, and the over-estimation at F3 is a result of an under-estimation of local spread, which accelerates rapidly between the ignition line and site F3.

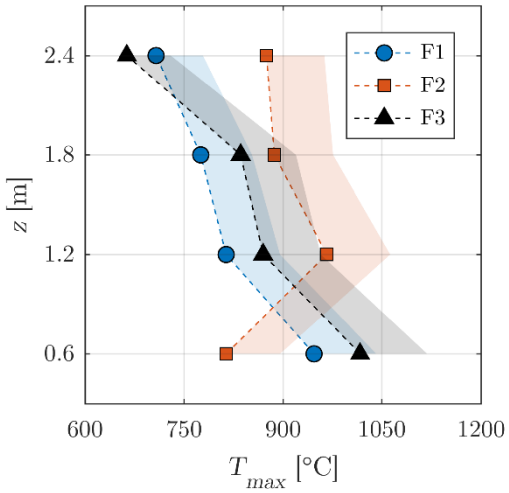

Fig. 6. Maximum instantaneous gas-phase temperature for each height at F1, F2, and F3. Shaded areas represent a maximum estimated temperature error of 10%.

These values are in a similar range to the findings of other field experiments which employed temperature measurement. For example, Wotten *et al.* [17] found a mean residence time of 37 s in a series of 77 surface fires of varying intensity in a eucalypt forest, with a standard deviation of 14 s. In five shrubland fires, Morandini and Silvani [16] report a residence time ranging from 21-31 s. Taylor *et al.* [11] reported mean residence times of 31-58 s in 10 crown fires, depending on thermocouple height, as well as an average 34 s from visual estimates. It must be noted that these comparisons are only useful as a means of providing general context for the values reported here. Given the differences in fuel types and environmental conditions investigated, strong agreement is not necessarily expected. However, they provide a useful point for comparison, particularly given the limited set of such measurements available in literature. This likewise applies to all subsequent discussion of previous field measurements.

Table 1. Flaming period characteristics for all thermocouple heights at the three sites. Measurements are peak temperature (T_g), residence time (t_r), and flame intermittency (Λ).

Site	h [m]	T_{max} [°C]	t_r [s]	Λ
F1	0.6	947	19.8	0.80
	1.2	814	21.2	0.62
	1.8	776	21.9	0.46
	2.4	708	17.7	0.67
F2	0.6	814	31.3	0.79
	1.2	966	33.9	0.67
	1.8	887	29.6	0.77
	2.4	875	29.5	0.77
F3	0.6	1017	27.8	0.88
	1.2	870	22.3	0.67
	1.8	836	17.4	0.75
	2.4	664	22.2	0.41

Flame intermittency (taken as the percentage of time when the measured temperature is in excess of 300 °C during the fire residence) is relatively constant along height in the crown fire, but shows an overall tendency to decrease for the surface fires (Table 1). However, in no case is the decrease purely monotonic, as might be expected. Typical discussions of intermittency have focused on well-defined fuel sources with a height less than the flame height under statistically steady (non-spreading)

conditions [35–38]. Therefore, applying classical theory to the flame region presents challenges, and investigation of flame structure in such complex forest fuels is of future interest.

3.3. Velocity

The magnitude of vertical velocity (w) can give an indication of the buoyancy forces, and is plotted for F1 and F2 in Fig. 7. The signals are noisy, but applying a 1-second moving average filter reveals that the value is essentially zero preceding the fire front arrival, as expected. Vertical velocity increases as the fire front arrives, reaching peak instantaneous maximums of 13.0 $m \cdot s^{-1}$ and 9.6 $m \cdot s^{-1}$ for F1 and F2, respectively. However, the flow is highly turbulent, with downdrafts in excess of 8.0 $m \cdot s^{-1}$ occurring at both sites. The residence of the fire at the primary tower (hatched area in Fig. 7) shows that significant vertical velocities are observed at almost the same time at the secondary tower at F1, while there is a delay at F2. This is consistent with the description of F1 having leaning/bursting flames which may impinge on the secondary tower even as the fire arrives at the primary tower. Following the fire front passage, the mean velocity quickly returns to near-zero, but the turbulent fluctuations are significantly enhanced by a combination of the intermittent flaming, smoldering combustion, and residual surface heat.

As mentioned previously, in-situ measurement of velocities within wildland fire flames does not appear frequently in literature. However, there are a few comparison points available. In an experimental grassland fire, Clements *et al.* [15] measured peak vertical velocities of ~10 $m \cdot s^{-1}$ near the surface (2.0 m), with downdrafts of ~5 $m \cdot s^{-1}$. For low-intensity grassland fires, Butler *et al.* [18] reported vertical velocities up to ~5 $m \cdot s^{-1}$ at a height of 0.5 m, with downdrafts reaching ~4 $m \cdot s^{-1}$. These values are in a similar order of magnitude range to those measured here, though they are closer to the experiment conducted by Clements *et al.* [15]. This makes sense as the intensity was greater than that in the experiment conducted by Butler *et al.* [18], potentially by as much as 5-10 times, locally.

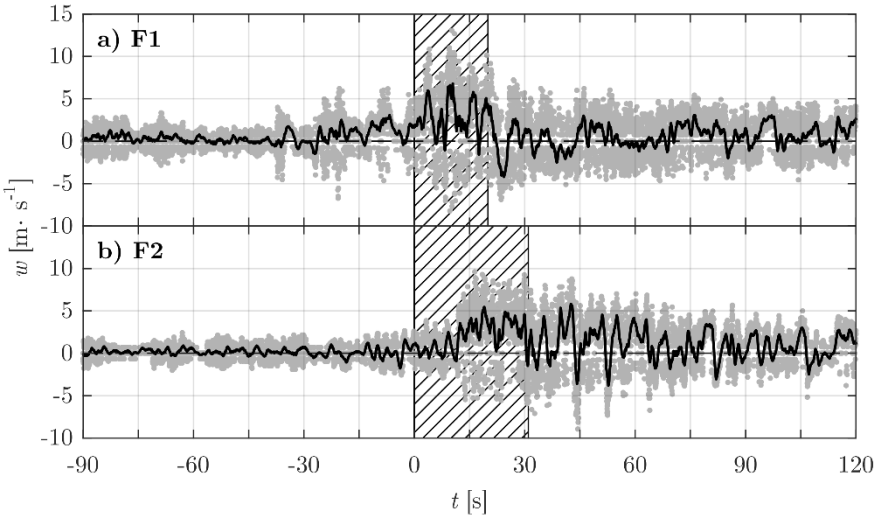

Fig. 7. Vertical velocity, with positive values representing upward flow and negative downward, for site (a) F1 and (b) F2. Filtered responses (1-second moving average) are plotted over raw data. Hatched regions show the un-shifted time of residence determined for the respective primary towers, 2 m upstream.

Axisymmetric plume theory shows that the magnitude of the buoyancy-driven vertical velocity will vary along height, increasing in the persistent flame to a maximum value in the intermittent flame, and then decaying again in the plume region [35]. Similar results have been found for line burners [39], which are more applicable to a fireline. While the three regions are difficult to identify in this case, as discussed previously, the measured values may have some dependence on sensor height. For example, if the probe at F2 is in the continuous flame region, where temperature does not vary much,

velocity should increase with height $\propto z^{0.5}$. However, these point measurements are valuable for qualitative assessment and providing data for model comparison.

The horizontal velocity measurements from the north/south facing pressure probe (v), are also important, as this was oriented in approximately the direction of fire approach for both F1 and F2. These measurements can be viewed in context of the ambient surface wind measurement which was made just outside the plot, to the north [21]. Horizontal wind here had an average value of 0.9 m·s^{-1}, from the north-northwest. While this measurement was made at a height of 3 m, it is indicative of the ambient wind which would be expected at the sites.

Fig. 8 shows a section of this data centered on the arrival of the fire front at each site. During the preheating stage, a reversal of flow direction occurs in the lee of the fire front. This is seen as northward (negative) flow which is counter to the aforementioned ambient wind and, therefore, indicative of entrainment flow. At the time of ignition, both sensors show small values fluctuating about zero, but this coherent northward flow manifests approximately 240 s before the fire arrives at F1 and 360 s before arriving at F2. Given the fact that temperatures remain low until the fire front is very close (Fig. 5) this flow should be associated with convective cooling of fuel particles. However, a few short bursts of air in the direction of fire spread are observed in the lead-up to the fire arrival at F1, with the first occurring around 35 s before the arrival of the fire. While these gusts are short-lived, they have magnitudes between 4.2 m·s^{-1} and 8.1 m·s^{-1} and may be linked to 'long-range' convective heating. This behavior is absent at F2, which is consistent with the description of taller, more upright flames resulting in a greater entrainment/sheltering effect.

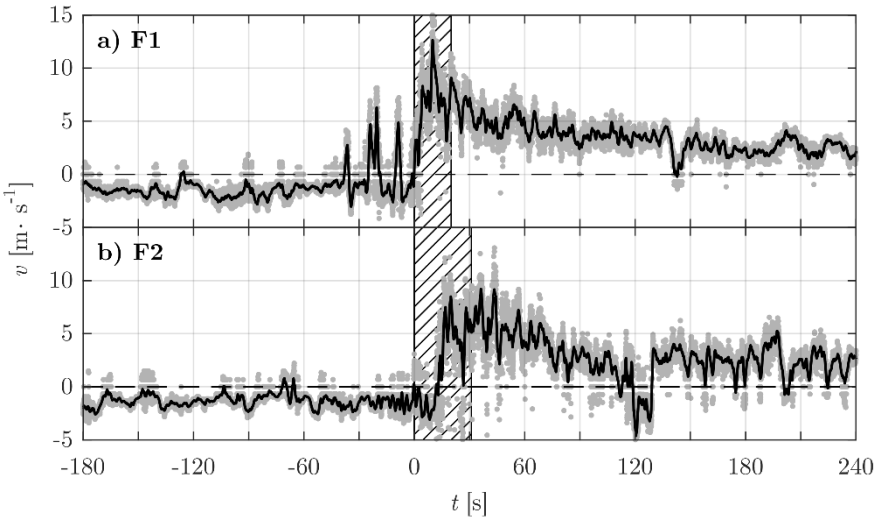

Fig. 8. Horizontal velocity in the north/south direction, with positive values representing flow to the south (the direction of fire spread), for site (a) F1 and (b) F2. Filtered responses (1-second moving averages) are plotted over raw data. Hatched regions show the un-shifted time of residence determined for the respective primary towers, 2 m upstream.

A difference in the role of convection for different fire intensities has been identified previously by Frankman *et al.* [9]. Their measurements suggest that convective preheating played a more significant role for lower intensity surface fires than for high-intensity crown fires. This difference in convection ahead of the fire agrees with the flow patterns observed here. Further, Finney et al. [40] discuss the importance of convective heat transfer in sustaining fire spread. The measurements of a flow reversal agree with their suggestion that convective cooling mechanisms can play an important role during long range preheating. As for the exact role of convective heating in ignition, it is difficult to separate the phenomena here, and detailed measurements of representative fuel particles may be of interest in future.

Following the arrival of the fire, the buoyancy driven flow of the fire has a strong horizontal effect at the surface level, with peak values of 16.2 $m \cdot s^{-1}$ and 13.1 $m \cdot s^{-1}$ for F1 and F2, respectively. The clear peak at F1 versus the more prolonged region of elevated velocity at F2 mirror the previous discussion of temperature. The flow within the flames themselves transitions to a strong, turbulent draft in the wake of the fire front, for both F1 and F2. This draft is believed to be an important mechanism contributing to the lofting of firebrands [41] and will also influence the intermittent-flaming and smoldering combustion of fuels in the wake of the fire.

In the grassland fire experiment of Clements *et al.* [15] horizontal fire-induced drafts of up to ~10 $m \cdot s^{-1}$ were measured at a height of 2.0 m (2-3 times ambient). A flow reversal was noted ahead of the fire front, but only for a brief period of ~50 s. Butler *et al.* [18] measured horizontal velocities up to ~9 $m \cdot s^{-1}$ in the direction of spread, and counter flows up to ~5 $m \cdot s^{-1}$ at a height of 0.5 m, though the timing of these with respect to the front was not discussed. The values obtained in this experiment are more consistent with the higher intensity grassland fires, however, there is a tendency for a more prolonged flow reversal ahead of the front and stronger draft flow. This may be related to differences in fire intensity, but the forest canopy may also play an important role. In both cases, the probes were situated above shrub height, and the canopy had a density on the order of 0.1 $kg \cdot m^{-3}$, with values increasing further with height (Fig. 4). This vegetation can help shelter the upwind region and promote a flow reversal, and the fire may also promote a sub-canopy wind jet in the wake region where vegetation density is significantly reduced compared to the canopy. This is particularly true given the effect of the fire in reducing bulk density close to the surface (Fig. 4). Such features warrant further investigation.

3.4. Radiative heat flux

Values of the convective heat transfer coefficient are obtained using Eq. (4). The range of h_c is consistent between the two sites, falling in the range of 12–34 $W \cdot m^{-2} \cdot K^{-1}$ and 11–24 $W \cdot m^{-2} \cdot K^{-1}$ for F1 and F2, respectively, during a two-minute period leading up to fire arrival. The slightly higher peak values for F1 corresponding to gusts ahead of the fire front in the last 30 seconds (Fig. 8).

The result of calculating the incident radiative heat flux from Equation 2 is shown in Fig. 9 for the TSCs at height of 1.1 m on the center secondary tower. As anticipated, a greater radiative flux was received at site F2. The peak value here is 52 $kW \cdot m^{-2}$, compared with 35 $kW \cdot m^{-2}$ at F1. Fig. 9a also reveals an earlier signal response at F1, with the value permanently exceeding 1 $kW \cdot m^{-2}$ as early as ~115 s before the arrival of the fire. This occurs at only ~60 s before arrival at F2. This may seem counterintuitive, given the more intense fire at F2, but this is due to the slower fire spread at F1. The fire was closer to the sensors at 115 s before arrival than it was at F2. Taking the local spread rates, this initial response corresponds to a consistent distance of 23 m and 24 m, respectively (Fig. 9b).

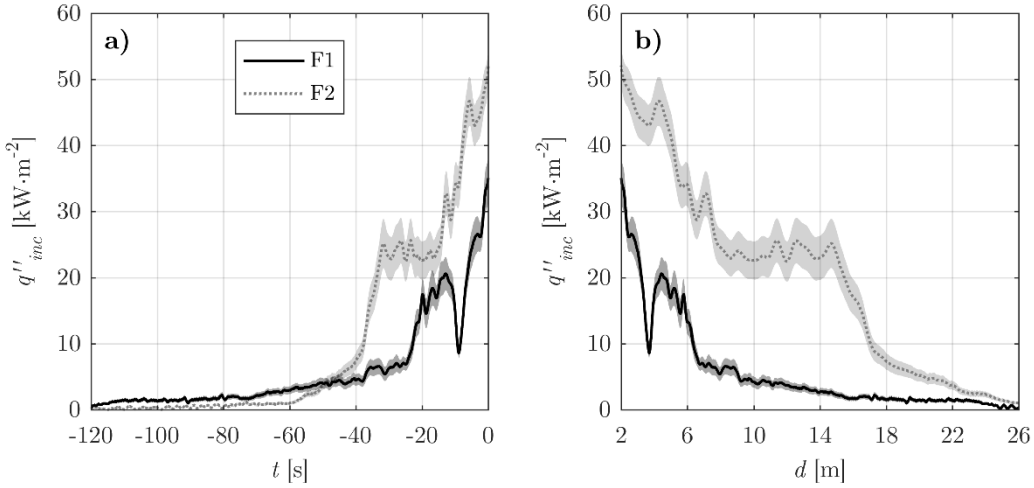

Fig. 9. Incident radiative heat flux, q''_{inc}, calculated for the TSC at z = 1.1 m on the center secondary tower for sites F1 and F2. x-axes represent (a) time to the fire arrival at the base of the primary tower and (b) distance to the heat flux sensor, estimated from the local spread rate. Shaded areas represent the two bounding assumptions (corrected and uncorrected) and the lines are an average of the two.

Context can be provided by examining other such measurements in field campaigns. In the preheating stage, Santoni *et al.* [14] found a peak radiative heat flux of 7.5 kW·m^{-2} at 5 m from the edge of an advancing shrubland fire (at a height of 2 m). Taking the local spread rates at F1 and F2, rough estimates of the 5 m heat flux here are 17 kW·m^{-2} and 41 kW·m^{-2}, respectively. This suggests a surface/shrub fire at F1, not unlike the shrub fire of Santoni *et al.* [14], particularly as the flux is changing rapidly at this point, so uncertainty in distance can mean a significant change in flux (the measurement is 7.5 kW·m^{-2} at ~6.5 m). However, a much more intense fire is observed at F2. At the time of fire front arrival in their shrubland experiments, Morandini and Silvani [16] reported radiative fluxes between ~15-50 kW·m^{-2}, making the values here consistent with their more intense fires. They also show initial responses 10-20 m from the fire front, again consistent with the values here. As this discussion only considers the preheating stage up to the primary towers, peak radiative fluxes should be even greater. As an example, Frankman *et al.* [9] reported peak radiative fluxes 120-132 kW·m^{-2} for brush fires and 189-300 kW·m^{-2} for crown fires. Finally, it is also interesting to note the apparent autoignition of a tree boles captured in video footage at F2. Such behavior has also been described in the International Crown Fire Modeling Experiment (ICFME), where vapor was observed to be released from tree boles, followed by ignition 3-4 m ahead of the fire front [11].

While the fire ended up approaching with the fireline roughly parallel to the face of the TSCs on the center towers at both F1 and F2, the sensors on the other towers were at significant angles (precise measurements of this angle were obtained in the field). Thus, the ability of the sensor to 'view' the fire must be evaluated. For wildland fires, such considerations are generally made for parallel surfaces of finite dimensions [13,42–45], but usually do not consider an angle. Further, the absolute view factor, which is typically solved for, is not of interest (as we are not trying to model radiation from the flame). Rather, a corrective factor is needed to account for the discrepancy between a parallel and oblique measurement.

To establish a correction factor, the fundamental equation describing the fraction of radiation leaving one surface i and arriving at another surface j, known as the view factor, is used. A simplification is introduced by taking the TSC disk to be a differential element (much smaller than the fire front) [10]:

$$F_{ij} = \frac{A_j}{A_i} \int \frac{\cos^2 \beta}{\pi r^2} dA_i, \tag{5}$$

where β is the angle between the normals of a point on the fire front and the sensor, and r is the distance between the two. Further, we assume the fire front has infinite length (a reasonable assumption given the length of the experimental fire compared to the size of the TSC); the flame height is H; the TSC is located at a fraction of this, aH (it is below flame height, so $0 \leq a \leq 1$); and the fire is a distance D from the TSC. This configuration is shown in Fig. 10. The equation can then be solved analytically for these geometric constraints [33]. Further, it is normalized against the solution where β =0 (giving F^*, the change in view factor as the sensor is angled away from the fire), and the variable α is introduced to describe the ratio between fire height and distance to sensor (H/D). Finally, we consider two bounding cases of sensor height which, due to symmetry, are when the sensor is at mid-flame height (a = 0.5) or the sensor is at the bottom or top edge of the flame (a = 0,1). This yields the following equations, respectively:

$$F^* = \frac{\cos\beta}{2} + \frac{2\sqrt{1+\alpha^2/4}}{\pi\alpha}\tan^{-1}\left(\frac{\alpha}{2}\sin\beta\right) + \frac{\cos\beta}{\pi}\tan^{-1}\left(\frac{\cot\beta}{\sqrt{1+\alpha^2/4}}\right), \quad (6)$$

$$F^* = \frac{\cos\beta}{2} + \frac{\sqrt{1+\alpha^2}}{\pi\alpha}\tan^{-1}(\alpha\sin\beta) + \frac{\cos\beta}{\pi}\tan^{-1}\left(\frac{\cot\beta}{\sqrt{1+\alpha^2}}\right). \quad (7)$$

An important result is that for an infinitely tall fire front ($\alpha \to \infty$) both equations collapse to $F^* = (\cos\beta + 1)/2$, which is the solution for a differential element in front of an infinite plane [46].

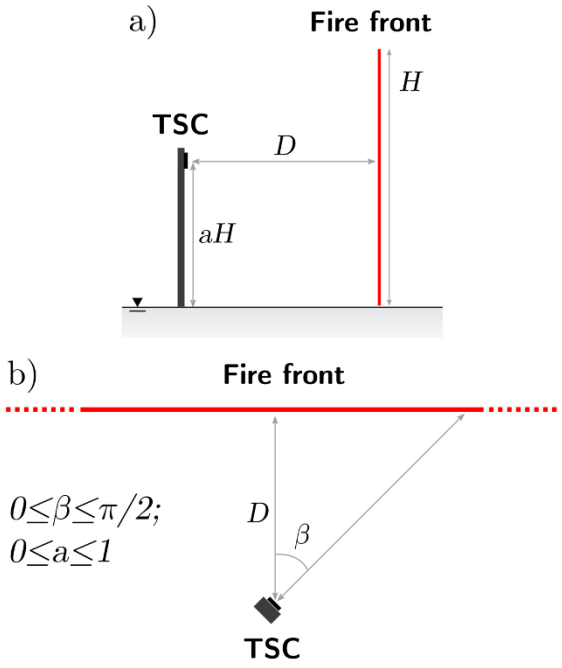

Fig. 10. a) Section and b) plan view of the theoretical orientation of the sensor and flame front.

Some example values of F^* are given in Fig. 11. This shows that the angle, β, is the dominant factor, with a perpendicular viewing angle ($\pi/2$) reducing the received radiation to ~30 – 40% of the zero-angle value, though small adjustments around zero have a less significant influence, as evidenced by the drop in $\partial F^*/\delta\beta$ for $\beta < \pi/8$. Furthermore, the effect on the correction of sensor position with respect to the flame height is negligible for small values of α. As this value increases, the influence of the height becomes more pronounced. However, it is still minor compared to the angle. For α = 2, at the maximum angle of $\beta = \pi/2$, F^* changes by ~10% between the two bounding values of a.

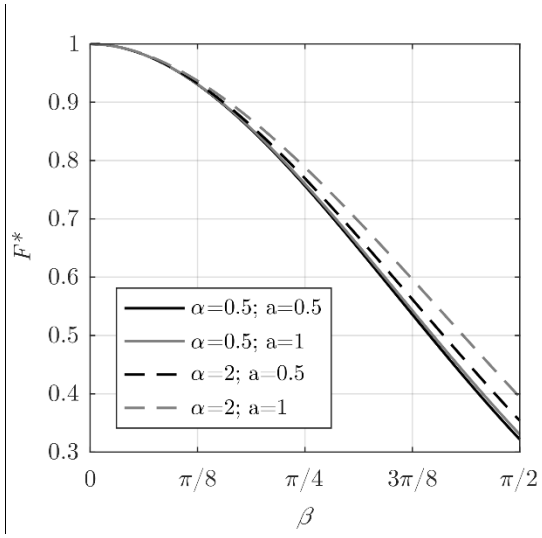

Fig. 11. Examples of view factor corrections for different flame height to distance ratios (α = 0.5, α = 2) and different sensor heights (a = 0.5, Equation (6); a = 1, Equation (7)).

Further improvements could be made to this approach by considering a flame tilt angle. A number of studies have discussed the effects of flame angle for radiation, though these have largely considered the flux to a horizontal fuel bed (e.g. [37,47–49]), finding that the value can double at maximum flame inclination [48]. One study considered the effect on forward radiation (to a vertical surface) [34], however, the reported test results included too many other variables to isolate the role of angle alone. Importantly, however, we are presently more interested in whether flame tilt angle will influence the correction for sensor angle. Fig. 11 shows that sensor height relative to the flame and flame distance do not play a large role in this correction, and a tilted flame when viewed straight on can be approximated by a shorter flame (particularly when it is further away so that the distance of forward flame projection is small compared to the distance to the sensor). Therefore, it can be assumed that flame tilt angle can be reasonably excluded from this first approximation of the correction factor.

In order to calculate the correction factor, F^*, for the experimental data, a determination of a, α, and β must be made. Concerning a, it is assumed that the sensors at F1 were closer to the top of the flames, while those at F2 were closer to the mid-flame height. Therefore, Eq. (6) and Eq. (7) are used for the two sites, respectively. The ratio α will change with time, as the fire approaches. Given the local spread rates, over the two-minute window of interest, $0.05 \leq \alpha \leq 0.6$ for F1, and $0.48 \leq \alpha \leq 1.2$ for F2. β was determined from an analysis of both the aerial IR imagery (Fig. 1) and an analysis of video footage (e.g. Fig. 3), using detailed maps of tree locations. Values are given in Table 2.

Table 2. Angle of fire approach, θ_F, measured clockwise from north, and view angle, β, based on sensor orientation, for each of the secondary towers (left, center, and right). Fire approach angle was determined from a combination of video analysis and the aerial IR imagery.

Site	θ_F [°]	β_L [°]	β_C [°]	β_R [°]
F1	173	40	13	51
F2	168	33	10	44

In order to compare the data from all TSCs in a more concise manner, the total incident radiative flux, Q''_{inc}, is obtained by integrating over the 120 s window (Fig. 12). This integration confirms a distinct difference in radiation between the two sites. The corrected measurements show Q''_{inc} to be ~1.7-1.8 times greater at F2 compared to F1.

The scatter in the uncorrected values of integrated flux at a given site (Fig. 12a) is revealed as largely an effect of sensor angle. Taking, as an example, the measurements at 1.1 m, applying the view angle

correction reduces the spread in measurement by 67% and 60% for F1 and F2, respectively (Fig. 12b). It should be mentioned that part of the scatter which remains is due to the fact that, as the fire did not approach the measurement sites head-on ($\beta_L = 0$), the towers were at different distances to the fire front at any given time. This is most significant at short distances, due to the inverse-square dependency of radiant intensity on distance (e.g., Eq. (5)), and is somewhat limited in this instance by only considering the time up to the arrival of the fire at the 'primary' tower. However, it can still be seen in the higher values for $F2_R$ after correction (as this tower was closest to the fire front at its oblique arrival). The fact that the sensors, when corrected, receive such consistent quantities of energy at a particular location demonstrates the relative robustness of radiative heat flux measurements in field experiments, given the high levels of heterogeneity and uncertainty involved. Temperature, velocity, and thus convective flux, can vary significantly with only a small change in sensor position. However, hemispherical radiant heat flux sensors integrate the energy over the area of the flame and are less sensitive to small changes position changes within a given site [9].

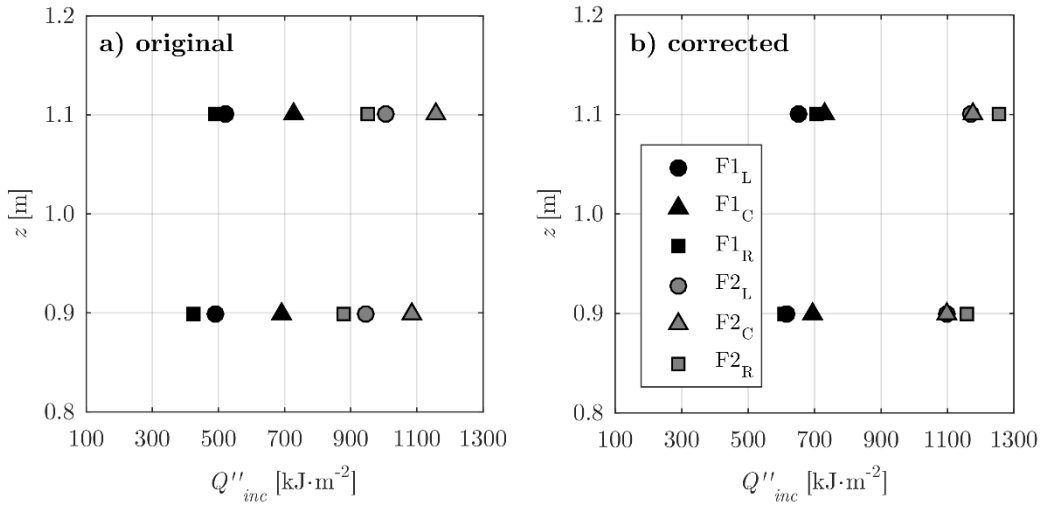

Fig. 12. (a) Uncorrected and (b) view-angle corrected integral incident radiative flux, Q''_{inc}, for sites F1 and F2. Values are integrated over a 120 s window, ending at the fire arrival at the 'primary' tower. Subscripts refer to the Left, Center, and Right 'secondary' towers.

Taking the view angle into account is significant, given the fact that radiative heat fluxes from field experiments are often reported without consideration of the relative approach angle of the fire. This is understandably difficult to quantify, as fires in the field are subject to localized, heterogeneous behavior and so it is usually not possible to fully prescribe this beforehand. Therefore, a good means of observing the actual approach of the fire is important, whether it is IR-based tracking of the fire front, visual cameras, or some other method. Without this, it becomes difficult to interpret experimental information and make one-to-one comparisons with, for example, predictions of a numerical model.

4. Conclusions

The local measurements of fire dynamics obtained from this field experiment help to quantify the macroscopic behavior observed. Characterization of the differences in the physical phenomena at the specific sites is of interest, more than the specific values of any one quantity. This is particularly the case given that both surface fire behavior (F1 and F3) and crown fire behavior (F2) were captured. These differences can be summarized as:

- Tall upright flames were observed in the region of crown fire (F2) compared with shorter flames in the region of surface fire (F1 and F3). This corresponded to greater flame residence times and intermittency at heights above the shrub layer for the crown fire (F2).

- A flow reversal in the region downwind of the fire (or sheltering) was observed in both cases. This persisted even immediately ahead of the crown fire arrival (F2), suggesting a limited extent to convective preheating, while the surface fire (F1) exhibited clear bursts of flow in the direction of spread.
- Radiative preheating was observed in both cases, up to about 25 m from the fire front, but integrated preheating was about 1.75 times greater in the crown fire region (F2) compared to the surface fire (F1).

These differences show the range of what may occur in this environment under relatively constant ambient conditions. The assessment of pre-fire fuel structure presented here, along with that in Mueller et al. [21], demonstrates that the mere presence of canopy fuels which are capable of supporting crown fire behavior is not alone sufficient for this behavior, and so the arrangement of surface fuels and/or local wind gusts must also important.

The observations of local fire dynamics described here can be directly compared to the predictions of a numerical model, particularly detailed physics-based models which aim to resolve such phenomena. Model testing through second-order descriptors of fire behavior (such as spread rate) is useful, but the accumulation of model errors in the representation of multiple fundamental processes may interact to produce an apparently correct result. This makes clear the importance of a combination of broad and detailed measurements over a range of scales. However, employing such detailed experimental measurements for model testing requires a thorough assessment of measurement limitation and uncertainty. In this case, considerations such as radiation errors for the thermocouples and the view angle correction to radiation measurements help to improve the robustness of the provided measurements as comparison points for a numerical model.

Ultimately, the presented methodology has been shown to be used successfully to quantify fire behavior processes. This is able to provide insight into the mechanisms that drive spread. Future improvements may include: taller thermocouple towers, to ensure the full extent of the flaming region can be captured; more sensitive pressure transducers, both in terms of accuracy at low velocity and response time for high-frequency fluctuations; and generally increased deployment of measurement sites across a burn area.

5. Nomenclature

A	surface area [m]
a	sensor height (as a proportion of flame height)
C	TSC conduction correction factor
c_p	specific heat [kJ·kg^{-1}·K^{-1}]
D	sensor distance [m]
F^*	normalized view factor
g	gravitational acceleration [m·s^{-2}]
H	flame height [m]
h_c	convective heat transfer coefficient [W·m^{-2}·K^{-1}]
K	pressure probe correction factor
k	thermal conductivity [W·m^{-1}·K^{-1}]
L	characteristic length scale [m]
m	mass [kg]
$\overline{Nu}_L$	average Nusselt number
P	pressure [Pa]

Pr	Prandtl number
Q''_{inc}	integral incident radiative heat flux [kJ·m^{-2}]
q''_{inc}	incident radiative heat flux [kW·m^{-2}]
Ra_L	Rayleigh number
Re_L	Reynolds number
t	time [s]
v	north/south velocity [m·s^{-1}]
w	vertical velocity [m·s^{-1}]
α	absorptivity, flame height to sensor distance ratio, thermal diffusivity [m^2·s^{-1}]
β	angle between sensor and fire front normal [°]
γ	TSC transient correction factor
ε	emissivity
θ_F	fire approach angle [°]
ν	kinematic viscosity [m^2·s^{-1}]
ρ	density [kg·m^{-3}]
σ	Stefan–Boltzmann constant [W·m^{-2}·K^{-4}]
Subscripts	
C,L,R	sensor location (center, left, right)
f	film
g	gas-phase
s	solid-phase
∞	ambient

6. Acknowledgements

The authors wish to thank the Joint Fire Science Program (JFSP) for funding this research effort (project #12-1-03-11), and the New Jersey Forest Fire Service, particularly Section Firewarden Ashley House, for their strong support in the planning and execution of the experimental fire. The authors also thank Dr. Kenneth Clark and Dr. Michael Gallagher who were instrumental in collecting meteorological and fuels data for the experiment.

7. References

[1] D. Morvan, Physical phenomena and length scales governing the behaviour of wildfires: A case for physical modelling, Fire Technol. 47 (2011) 437–460.

[2] M.E. Alexander, M.G. Cruz, Are the applications of wildland fire behaviour models getting ahead of their evaluation again?, Environ. Model. Softw. 41 (2013) 65–71.

[3] D. Ward, Combustion chemistry and smoke, in: For. Fires Behav. Ecol. Eff., Academic Press, San Diego, 2001: pp. 55–77.

[4] W.M. Pitts, E. Braun, R.D. Peacock, H.E. Mitler, E.L. Johnsson, P.A. Reneke, L.G. Blevins, Temperature uncertainties for bare-bead and aspirated thermocouple measurements in fire environments, in: Therm. Meas. Found. Fire Stand., ASTM International, West Conshohocken, PA, 2003.

[5] W.M. Pitts, Wind effects on fires, Prog. Energy Combust. Sci. 17 (1991) 83–134.

[6] B.E. Potter, Atmospheric interactions with wildland fire behaviour–I. Basic surface interactions, vertical profiles and synoptic structures, Int. J. Wildl. Fire. 21 (2012) 779–801.

[7] B.E. Potter, Atmospheric interactions with wildland fire behaviour–II. Plume and vortex dynamics, Int. J. Wildl. Fire. 21 (2012) 802–817.

[8] H.E. Anderson, Heat transfer and fire spread, USDA Forest Service, Intermountain Forest and Range Experimental Station, Ogden, Utah, 1969.

[9] D. Frankman, B.W. Webb, B.W. Butler, D. Jimenez, J.M. Forthofer, P. Sopko, K.S. Shannon, J.K. Hiers, R.D. Ottmar, Measurements of convective and radiative heating in wildland fires, Int. J. Wildl. Fire. 22 (2013) 157–167.

[10] F.P. Incropera, D.P. DeWitt, T.L. Bergman, A.S. Lavine, Fundamentals of heat and mass transfer, John Wiley & Sons, 2007.

[11] S.W. Taylor, B.M. Wotton, M.E. Alexander, G.N. Dalrymple, Variation in wind and crown fire behaviour in a northern jack pine black spruce forest, Can. J. For. Res. 34 (2004) 1561–1576.

[12] B.W. Butler, J. Cohen, D.J. Latham, R.D. Schuette, P. Sopko, K.S. Shannon, D. Jimenez, L.S. Bradshaw, Measurements of radiant emissive power and temperatures in crown fires, Can. J. For. Res. 34 (2004) 1577–1587.

[13] J.D. Cohen, Relating flame radiation to home ignition using modeling and experimental crown fires, Can. J. For. Res. 34 (2004) 1616–1626.

[14] P.A. Santoni, A. Simeoni, J.L. Rossi, F. Bosseur, F. Morandini, X. Silvani, J.H. Balbi, D. Cancellieri, L. Rossi, Instrumentation of wildland fire: Characterisation of a fire spreading through a Mediterranean shrub, Fire Saf. J. 41 (2006) 171–184.

[15] C.B. Clements, S. Zhong, S. Goodrick, J.P. Li, X. Bian, W.E. Heilman, J.J. Charney, R. Perna, M. Jang, D. Lee, Observing the dynamics of wildland grass fires: FireFlux-a field validation experiment, Bull. Am. Meteorol. Soc. 88 (2007) 1369–1382.

[16] F. Morandini, X. Silvani, Experimental investigation of the physical mechanisms governing the spread of wildfires, Int. J. Wildl. Fire. 19 (2010) 570–582.

[17] B.M. Wotton, J.S. Gould, W.L. McCaw, N.P. Cheney, S.W. Taylor, Flame temperature and residence time of fires in dry eucalypt forest, Int. J. Wildl. Fire. 21 (2012) 270–281.

[18] B. Butler, C. Teske, D. Jimenez, J. O'Brien, P. Sopko, C. Wold, M. Vosburgh, B. Hornsby, E.L. Loudermilk, Observations of energy transport and rate of spreads from low-intensity fires in longleaf pine habitat-RxCADRE 2012, Int. J. Wildl. Fire. 25 (2016) 76–89.

[19] M.G. Cruz, B.W. Butler, D.X. Viegas, P. Palheiro, Characterization of flame radiosity in shrubland fires, Combust. Flame. 158 (2011) 1970–1976.

[20] C.B. Clements, B. Davis, D. Seto, J. Contezac, A. Kochanski, J.-B. Fillipi, N. Lareau, B. Barboni, B. Butler, S. Krueger, Overview of the 2013 FireFlux II grass fire field experiment, in: Adv. For. Fire Res. - Proc. 7th Int. Conf. For. Fire Res., University of Coimbra: Coimbra, Portugal, 2014: pp. 392–400.

[21] E. V. Mueller, N. Skowronski, K. Clark, M. Gallagher, R. Kremens, J.C. Thomas, M. El Houssami, A. Filkov, R.M. Hadden, W. Mell, A. Simeoni, Utilization of remote sensing techniques for the quantification of fire behavior in two pine stands, Fire Saf. J. 91 (2017) 845–854.

[22] X. Silvani, F. Morandini, Fire spread experiments in the field: Temperature and heat fluxes measurements, Fire Saf. J. 44 (2009) 279–285.

[23] B.J. McCaffrey, G. Heskestad, A robust bidirectional low velocity probe for flame and fire application, Combust. Flame. 26 (1976) 125–127.

[24] C.Y. Liu, Y.W. Wong, W.K. Chan, T.C. Can, Note on the robust bidirectional low velocity probe, Exp. Fluids. 9 (1990) 354–356.

[25] ASTM International, ASTM E459 - 05: Standard test method for measuring heat transfer rate using a thin-skin calorimeter, ASTM International, West Conshohocken, PA, 2011.

[26] J.P. Hidalgo, C. Maluk, A. Cowlard, C. Abecassis-Empis, M. Krajcovic, J.L. Torero, A Thin Skin Calorimeter (TSC) for quantifying irradiation during large-scale fire testing, Int. J. Therm. Sci. 112 (2016) 383–394.

[27] M.J. Gollner, X. Huang, J. Cobian, A.S. Rangwala, F.A. Williams, Experimental study of upward flame spread of an inclined fuel surface, Proc. Combust. Inst. 34 (2013) 2531–2538.

[28] A.H. Majdalani, J.E. Cadena, A. Cowlard, F. Munoz, J.L. Torero, Experimental characterisation of two fully-developed enclosure fire regimes, Fire Saf. J. 79 (2016) 10–19.

[29] A. Amundarain, Assessment of the thermal efficiency, structure and fire resistance of lightweight building systems for optimized design, PhD Thesis, University of Edinburgh, School of Engineering, 2007.

[30] S.L. Manzello, S.-H. Park, T.G. Cleary, Development of rapidly deployable instrumentation packages for data acquisition in wildland–urban interface (WUI) fires, Fire Saf. J. 45 (2010) 327–336.

[31] E.A. Sullivan, A.G. McDonald, Mathematical model and sensor development for measuring energy transfer from wildland fires, Int. J. Wildl. Fire. 23 (2014) 995–1004.

[32] N.D. Burrows, Flame residence times and rates of weight loss of eucalypt forest fuel particles, Int. J. Wildl. Fire. 10 (2001) 137–143.

[33] E. V Mueller, Examination of the underlying physics in a detailed wildland fire behavior model through field-scale experimentation, University of Edinburgh, 2016.

[34] A.L. Sullivan, P.F. Ellis, I.K. Knight, A review of radiant heat flux models used in bushfire applications, Int. J. Wildl. Fire. 12 (2003) 101–110.

[35] B.J. McCaffrey, Purely buoyant diffusion flames: some experimental results, National Bureau of Standards, National Engineering Laboratory, Center for Fire Research, Washington, DC, 1979.

[36] J.-L. Dupuy, J. Marechal, D. Morvan, Fires from a cylindrical forest fuel burner: combustion dynamics and flame properties, Combust. Flame. 135 (2003) 65–76.

[37] F. Morandini, A. Simeoni, P.-A. Santoni, J.-H. Balbi, A model for the spread of fire across a fuel bed incorporating the effects of wind and slope, Combust. Sci. Technol. 177 (2005) 1381–1418.

[38] M.E. Schneider, L.A. Kent, Measurements of gas velocities and temperatures in a large open pool fire, Fire Technol. 25 (1989) 51–80.

[39] L.-M. Yuan, G. Cox, An experimental study of some line fires, Fire Saf. J. 27 (1996) 123–139.

[40] M.A. Finney, J.D. Cohen, J.M. Forthofer, S.S. McAllister, M.J. Gollner, D.J. Gorham, K. Saito, N.K. Akafuah, B.A. Adam, J.D. English, Role of buoyant flame dynamics in wildfire spread, Proc. Natl. Acad. Sci. 112 (2015) 9833–9838.

[41] M. El Houssami, E. V Mueller, A. Filkov, J.C. Thomas, N. Skowronski, M.R. Gallagher, K. Clark, R. Kremens, A. Simeoni, Experimental Procedures Characterising Firebrand Generation

in Wildland Fires, Fire Technol. 52 (2015) 731–751.

[42] B.W. Butler, J.D. Cohen, Firefighter safety zones: a theoretical model based on radiative heating, Int. J. Wildl. Fire. 8 (1998) 73–77.

[43] L. Zárate, J. Arnaldos, J. Casal, Establishing safety distances for wildland fires, Fire Saf. J. 43 (2008) 565–575.

[44] F. Morandini, Y. Perez-Ramirez, V. Tihay, P.-A. Santoni, T. Barboni, Radiant, convective and heat release characterization of vegetation fire, Int. J. Therm. Sci. 70 (2013) 83–91.

[45] W. La Fons, H.B. Clements, E.R. Elliott, P.M. George, Project fire model, USDA Forest Service, Southeastern Forest Experiment Station, Southern Forest Laboratory, Macon, Georgia, 1962.

[46] M.F. Modest, Radiative heat transfer, Academic press, New York, 2013.

[47] P.J. Pagni, T.G. Peterson, Flame spread through porous fuels, Symp. Combust. 14 (1973) 1099–1107.

[48] P.G. Baines, Physical mechanisms for the propagation of surface fires, Math. Comput. Model. 13 (1990) 83–94.

[49] J.M.C. Mendes-Lopes, J.M.P. Ventura, J.M.P. Amaral, Flame characteristics, temperature-time curves, and rate of spread in fires propagating in a bed of Pinus pinaster needles, Int. J. Wildl. Fire. 12 (2003) 67–84.